Combustion Behavior of Algal Biochars Obtained at Different Pyrolysis Heating Rates

Vikul Vasudev, Xiaoke Ku,* and Jianzhong Lin

ACCESS | Metrics & More | Article Recommendations

ABSTRACT: In this work, the combustion performance of *Chlorella vulgaris* (CV), *Dunaliella salina* (DS), and *Haematococcus pluvialis* (HP) algal biochars was analyzed based on the multicomponent method. The biochars were obtained via nonisothermal pyrolysis of raw algal biomasses at three different heating rates (i.e., 30, 40, and 50 °C/min), and biochar combustion was performed from 200 to 700 °C at a heating rate of 5 °C/min. The complex oxidative reaction of algal biochar was resolved into combined reactions of multiple pseudo-components based on the peak deconvolution method using a bi-Gaussian model. The activation energies (E_a) for each pseudo-component (PC) of all biochar samples were calculated by the Coats−Redfern isoconversional method and four kinetic models (i.e., diffusion, nucleation, order-based, and shrinking core models). The results showed that the highest E_a values were predicted by the diffusion model. Except that the E_a for the first PC of CV biochar decreased by 16.45%, the E_a values for all other biochar samples generally increased with increasing the pyrolysis heating rate. Moreover, when the diffusion model was used, the E_a for the second PC of CV biochar increased by 50.87%, that for the first PC of DS biochar increased by 16.85%, and those for the first and third PCs of HP biochar increased by 4.66 and 11.66%, respectively. In addition, the combustibility index (S_n) was evaluated based on the ignition and burnout temperatures as well as the mean and maximum weight loss rates. Generally, the combustion performance of all biochar samples was good at a low temperature but deteriorated toward a high temperature. As the pyrolysis heating rate increases, an overall increase in the combustion quality was also seen for the second PC of CV biochar and the first PCs of DS and HP biochars because their S_n increased from 2.70×10^{-15} to 3.07×10^{-15} °C^{-5}, 2.53×10^{-13} to 3.88×10^{-13} °C^{-5}, and 3.00×10^{-13} to 3.26×10^{-13} °C^{-5}, respectively.
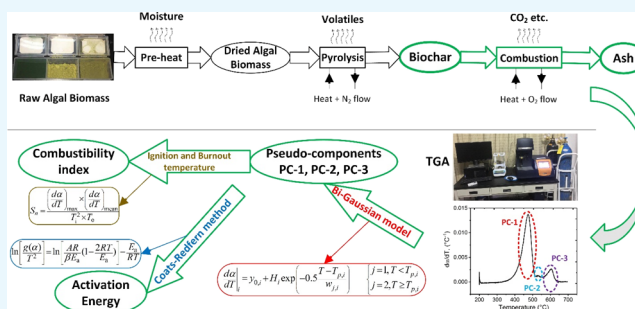
1. INTRODUCTION

Due to its abundance and carbon-neutral properties, biomass has been considered a renewable energy source with great potential.[1,2] The common lignocellulosic biomass (e.g., soybean, cottonseed, and agricultural and forest residues) is generally made up of three major biopolymers, i.e., hemicellulose, cellulose, and lignin.[3−5] Different from lignocellulosic biomass, algal biomass basically consists of carbohydrates, proteins, and lipids and has many intrinsic advantages, for example, short growth cycles, high yield per hectare, and the ability to grow in wastewater and saltwater.[6−8] All these factors make algal biomass more attractive than other types of biomass, although the technology that enables us to harness it efficiently is still in the early stage.[9,10]

Through thermochemical conversion, raw biomass can be transformed to high-quality energy products (e.g., bio-oil, syngas, and biochar) or just burned to release stored energy.[2] Among various conversion technologies, pyrolysis is a promising one during which biomass decomposition occurs under an inert environment, and multiple products, such as bio-oil and biochar, can be obtained. Bio-oil could be used in

fuel-related areas such as the jet fuel and automobile sectors.[11,12] Biochar has the ability to treat wastewater and is also used as a fertilizer for agricultural purposes or barbeque charcoal.[13,14] Koçer et al.[15] performed a parametric study on algal biochar yield obtained after pyrolysis. Elnour et al.[16] studied the effect of pyrolysis temperature on date palm biochar and the morphology of biochar/polypropylene composites. Pyrolysis is also the first process that occurs in many other thermochemical conversion routes (e.g., gasification and combustion).[5,17] Therefore, to optimize the reactor efficiency, it is necessary to fully understand the effect of pyrolysis operating conditions on the product yield.

Table 1. Properties of Raw Biomass Samples[d]

samples	C[a] (wt %)	H[a] (wt %)	N[a] (wt %)	O[a,c] (wt %)	S[a] (wt %)	moisture[b] (wt %)	VM[b] (wt %)	FC[b,c] (wt %)	ash[b] (wt %)	HHV[a] (MJ/kg)
CV	49.39 ± 0.46	7.27 ± 0.39	2.99 ± 0.14	39.32	1.03 ± 0.11	6.12 ± 0.39	73.79 ± 0.66	13.96	6.13 ± 0.18	21.252
DS	47.40 ± 0.56	6.69 ± 0.31	3.52 ± 0.09	40.99	1.40 ± 0.02	5.44 ± 0.50	73.99 ± 1.64	12.82	7.75 ± 0.28	19.708
HP	55.96 ± 0.54	7.96 ± 0.41	2.31 ± 0.01	33.20	0.57 ± 0.02	3.02 ± 0.23	81.31 ± 0.48	12.80	2.87 ± 0.07	25.001

[a]Dry ash-free basis. [b]As-received basis. [c]Calculated by difference. [d]Some data in our previous publication[3] are reused here with the permission from the Elsevier Publisher.

Knowledge of reaction kinetics helps in understanding biomass conversion behavior.[18,19] The most commonly used experimental apparatus for achieving this purpose is a thermogravimetric analyzer (TGA). Generally, a small quantity (5−20 mg) of a biomass sample is placed in a TGA and heated to a high temperature under different gas environments, and meanwhile, the weight loss is recorded.[4,20] To perform the kinetic analysis, three kinetic parameters, i.e., the activation energy, the pre-exponential factor, and the kinetic model equation, need to be evaluated. Two kinds of methods (i.e., differential and integral isoconversional methods) are normally used to determine these parameters, among which the Coats−Redfern method can use the data of a single nonisothermal experiment to evaluate the kinetic parameters and is suitable for a number of biomass samples.[21−24]

Biochar is an important product after pyrolysis, and its combustion is a complex process. If the reaction is considered a single-step process, it might be difficult to estimate the kinetic parameters precisely. Therefore, a multicomponent method is more suitable, and various functions (e.g., Frazer−Suzuki, Weibull, Lorentz, and bi-Gaussian) can be used to identify the components.[25−28] Hu et al.[25] performed a pyrolysis kinetic analysis of lignocellulosic biomasses using the deconvolution method and Frazer−Suzuki's model. They treated the biomass as a mixture of subcomponents, and separate kinetic parameters were evaluated for each sub-component. Sharma et al.[26] investigated the nonisothermal pyrolysis kinetics of biomass by resolving raw biomass into pseudo-components using the bi-Gaussian model. Moreover, many other studies were also found in the literature whose focus was on the pyrolysis kinetics of lignocellulosic and waste biomass samples.[29−32] However, to the best of our knowledge, few works have explored the effect of the pyrolysis heating rate on algal biochar combustion kinetics by resolving the feedstock into multiple pseudo-components.

In industrial-scale biomass combustion applications, pyrolysis is the precursor process that can influence the path of subsequent reactions. The biochar formed during pyrolysis can combust at high temperatures via several heterogeneous reactions.[33] Therefore, it is necessary to perform a parametric study on the effect of the pyrolysis heating rate on biochar yield and combustion performance. This study aims to analyze the difference in combustion behavior of algal biochars obtained at various pyrolysis heating rates. The obtained results will enhance the understanding of algal biochar combustion and how its pseudo-components decompose and react to the pyrolysis heating rate. The findings will also contribute to the optimization of operating parameters for performing efficient algal biomass conversion processes.

Specifically, we employed three algal biomass samples to study the effect of the pyrolysis heating rate on their biochar combustion performance. Biochar was produced using non-isothermal pyrolysis at three different heating rates (i.e., 30, 40,

and 50 °C/min). Thereafter, biochar combustion was performed from 200 to 700 °C at a heating rate of 5 °C/min under oxygen purging. The differential thermogravimetric curves of certain samples indicated that there were multiple pseudo-components that decomposed at different reaction stages. Thus, the peak deconvolution method was used to divide the whole combustion process into various stages using the bi-Gaussian function that incorporates the skewness of the peaks. To evaluate the activation energy of each pseudo-component (PC), the integral isoconversional method of Coats−Redfern was employed, which is frequently adopted in the literature, and a unique value of "apparent" activation energy can be obtained using only a single heating rate.[21] Since this method requires prior knowledge of the kinetic model equation, we adopted four different kinetic models, i.e., diffusion, order-based, nucleation, and shrinking core models, to calculate the activation energy individually. Furthermore, to assess the combustion performance, the combustibility index was calculated based on the estimated ignition and burnout temperatures as well as the mean and maximum weight loss rates. A systematic comparison between the results of different pseudo-components of all biochar samples was also made.

2. MATERIALS AND METHODS

2.1. Sample Details. Biomass samples from three algal species, *Chlorella vulgaris* (CV), *Dunaliella salina* (DS), and *Haematococcus pluvialis* (HP), were used. These intensively researched algal biomass species have unique properties. For example, CV has a remarkable carbon-capturing property and can be blended with coal for combustion.[34,35] DS is an industrially important biomass species because of its large-scale growth in high-salinity waters, and HP has a high astaxanthin content.[36,37] All these raw samples were purchased from WUDILVQI Bioengineering Co., Ltd. (China) in a powdered form, and Table 1 provides their properties. Note that the ultimate analysis was conducted based on the ASTM standard test method (i.e., ASTM E870-82), and the proximate analysis was carried out using the method proposed by Qin and Thunman.[30] The heating values (HHVs) were obtained by the following empirical correlation.[38]

$$HHV = 0.3443C + 1.192H - 0.113O - 0.024N + 0.093S \quad (1)$$

2.2. Experimental Methods. All thermogravimetric experiments were performed in a thermogravimetric analyzer (TGA), i.e., a TGA-55 (TA instruments, USA), with a sample size of approximately 12 mg. Initially, the raw samples inside the TGA furnace were dried by increasing the temperature up to 150 °C under nitrogen purging. After that, the pyrolysis process was carried out by increasing the temperature from 150 to 850 °C at three different heating rates (i.e., 30, 40, and 50 °C/min) under a nitrogen environment, and the holding time at 850 °C was 5 min. Note that these heating rates are

typical choices for obtaining biochar and are also frequently used in the literature.[30,39] After pyrolysis, the temperature was reduced to 200 °C, and the residual material was biochar. Then, the temperature was increased to 700 °C at a heating rate of 5 °C/min under an oxygen environment for biochar combustion.[30] The heating rate for the biochar combustion process was relatively low, resulting in a long residence time, which allowed a more complete reaction for the biochar samples. In addition, each experimental case was performed at least three times to ensure reproducibility.

2.3. Kinetic Modeling and Deconvolution of Data. Solid-state reactions are generally studied using the fractional conversion parameter α, which is defined as the normalized weight loss.

$$\alpha = \frac{m_0 - m}{m_0 - m_\mathrm{f}} \quad (2)$$

where m_0, m, and m_f are the initial, instantaneous, and final indecomposable masses of the sample during the reaction, respectively. Using α, the reaction rate is generally calculated by the following equation.[21]

$$\frac{d\alpha}{dt} = k(T)f(\alpha) = A\exp\left(-\frac{E_\mathrm{a}}{RT}\right)f(\alpha) \quad (3)$$

where $k(T)$ is the temperature-dependent Arrhenius function containing the activation energy E_a and the pre-exponential factor A. R is the universal gas constant, and $f(\alpha)$ is the kinetic model. Equation 3 can be written in integral form as

$$g(\alpha) = \int_0^\alpha \frac{d\alpha}{f(\alpha)} = \frac{AE_\mathrm{a}}{\beta R} \int_{y_\alpha}^\infty \frac{\exp(-y)}{y^2} dy \quad (4)$$

where $y = E_\mathrm{a}/RT$ and $y_\alpha = E_\mathrm{a}/RT_\alpha$ in which T_α is the temperature at a fixed α, and β is the constant heating rate. The Arrhenius integral on the right-hand side of eq 4 can be solved by integration by parts. The asymptotic expansion of this integral $p(y)$ can be written as[23]

$$p(y) = \frac{\exp(-y)}{y^2} \times \left(1 + \frac{2!}{-y} + \frac{3!}{(-y)^2} + \frac{4!}{(-y)^3} + \dots\right) \quad (5)$$

Coats and Redfern[22] made the approximation by adopting the first two terms of this series.

$$p(y) \cong \frac{\exp(-y)}{y^2}\left(1 - \frac{2}{y}\right) \quad (6)$$

Using this approximation, a linear equation can be written from eq 4 as

$$\ln\left[\frac{g(\alpha)}{T^2}\right] = \ln\left[\frac{AR}{\beta E_\mathrm{a}}\left(1 - \frac{2RT}{E_\mathrm{a}}\right)\right] - \frac{E_\mathrm{a}}{RT} \quad (7)$$

By plotting $\ln[g(\alpha)/T^2]$ against $1/T$, the activation energy E_a can be evaluated from the slope of the linear plot. Note that $g(\alpha)$ needs to be known beforehand for employing this method. For some samples, the biochar combustion process shows multiple peaks, indicating that different pseudo-components decompose at different temperatures. Such a complex combustion process cannot be described by a single model-fitting method.[40] The whole process can be treated as multiple independent parallel reactions such that the

combustion of each pseudo-component behaves like an individual reaction with its individual kinetic parameters. Therefore, the peak deconvolution of the whole data was performed based on the multiple peak fitting method. $d\alpha/dT$ of the ith pseudo-component can be defined using the bi-Gaussian function.[25,26,28]

$$\frac{d\alpha}{dT}\bigg|_i = y_{0,i} + H_i\exp\left(-0.5\frac{T - T_{\mathrm{p},i}}{w_{j,i}}\right)\begin{cases} j = 1, \, T < T_{\mathrm{p},i} \\ j = 2, \, T \geq T_{\mathrm{p},i} \end{cases} \quad (8)$$

where y_0, H, T_p, and w_j are the baseline, peak height, peak temperature, and half peak width, respectively. Therefore, the overall decomposition rate $d\alpha/dT$ containing n pseudo-components is

$$\frac{d\alpha}{dT} = \sum_{i=1}^n y_{0,i} + H_i\exp\left(-0.5\frac{T - T_{\mathrm{p},i}}{w_{j,i}}\right)\begin{cases} j = 1, \, T < T_{\mathrm{p},i} \\ j = 2, \, T \geq T_{\mathrm{p},i} \end{cases} \quad (9)$$

The unknown parameters in eq 9 were estimated by performing nonlinear regression using the Levenberg–Marquardt algorithm and minimization of the chi-square function.

$$\chi^2 = \frac{1}{n_\mathrm{eff} - p}\sum_{k=1}^{n_\mathrm{eff}} w_k\left(\frac{d\alpha}{dT}\bigg|_{k,\mathrm{EXP}} - \frac{d\alpha}{dT}\bigg|_{k,\mathrm{CALC}}\right)^2 \quad (10)$$

where n_eff is the total number of data points used in the fitting and p is the number of adjustable parameters. Note that this is a nonweighted approach; thus, w is treated as unity. A summary of the overall process, including deconvolution and kinetic modeling, is given in Figure 1.
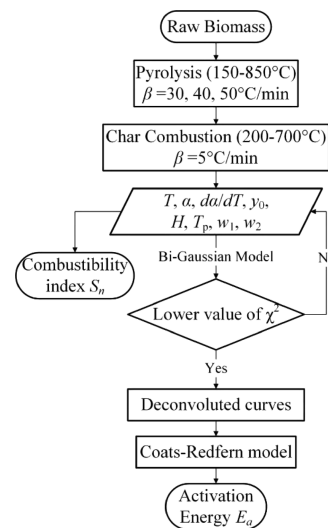

Figure 1. Flow chart of the kinetic analysis of algal biochar combustion.

3. RESULTS AND DISCUSSION

3.1. Biochar Yield and Combustion Characteristics. The pyrolysis heating rate plays an important role when determining the biochar yield. Table 2 lists the biochar yields obtained after pyrolysis of algal biomass samples at three different heating rates (i.e., 30, 40, and 50 °C/min).

Table 2. Biochar Yields Obtained at Different Pyrolysis Heating Rates

sample	heating rate (°C/min)	biochar yield (wt %)
CV	30	18.36 ± 2.09
	40	20.47 ± 4.11
	50	21.83 ± 1.89
DS	30	14.17 ± 3.44
	40	21.91 ± 5.56
	50	21.48 ± 2.52
HP	30	14.35 ± 1.33
	40	14.24 ± 2.54
	50	13.94 ± 2.02

Apparently, for CV and DS, the biochar yield increases with increasing the pyrolysis heating rate, probably because a quicker heating process means less residence time, which leads to an incomplete degradation at the end of the pyrolysis process. Koçer et al.[15] studied the biochar yield during pyrolysis and revealed that the biochar yield of CV increased with increasing the pyrolysis heating rate. However, for HP, a very slight decrease in the biochar yield is observed when increasing the heating rate. Angin[41] also found that at 600 °C, the biochar yield of safflower seeds dropped by 1.76% when increasing the pyrolysis heating rate from 10 to 50 °C/min.

Figure 2 shows the evolution curves of α and $d\alpha/dT$ with temperature T for the biochar combustion process. From the α curves, it is easily seen that the pyrolysis heating rate affects biochar combustion in different ways. For CV biochar, as the pyrolysis heating rate increases from 30 to 40 °C/min, the α evolution curve slightly shifts toward lower temperatures. However, when it further increases from 40 to 50 °C/min, no significant changes appear in the curves. For DS biochar, within the whole range tested, the α evolution curves continuously shift toward lower temperatures with an increase in the pyrolysis heating rate. For HP biochar, there seems to be no observable differences among the three pyrolysis heating rates investigated.

The $d\alpha/dT$ evolution curves presented in Figure 2 shed more light on the combustion behavior of these algal biochars, as multiple components can be observed decomposing at different stages.[42] For the CV and DS biochars, the whole combustion process could be divided into two different stages, as two distinct peaks are observed in the curves. For HP biochar, the reaction seems to be more complex due to the existence of three peaks at different temperatures. These peaks represent the reaction of pseudo-compounds that are probably formed during pyrolysis of raw biomass samples. Since these peaks are quite distinct, it is not good to treat the whole process as a single reaction. Therefore, each pseudo-
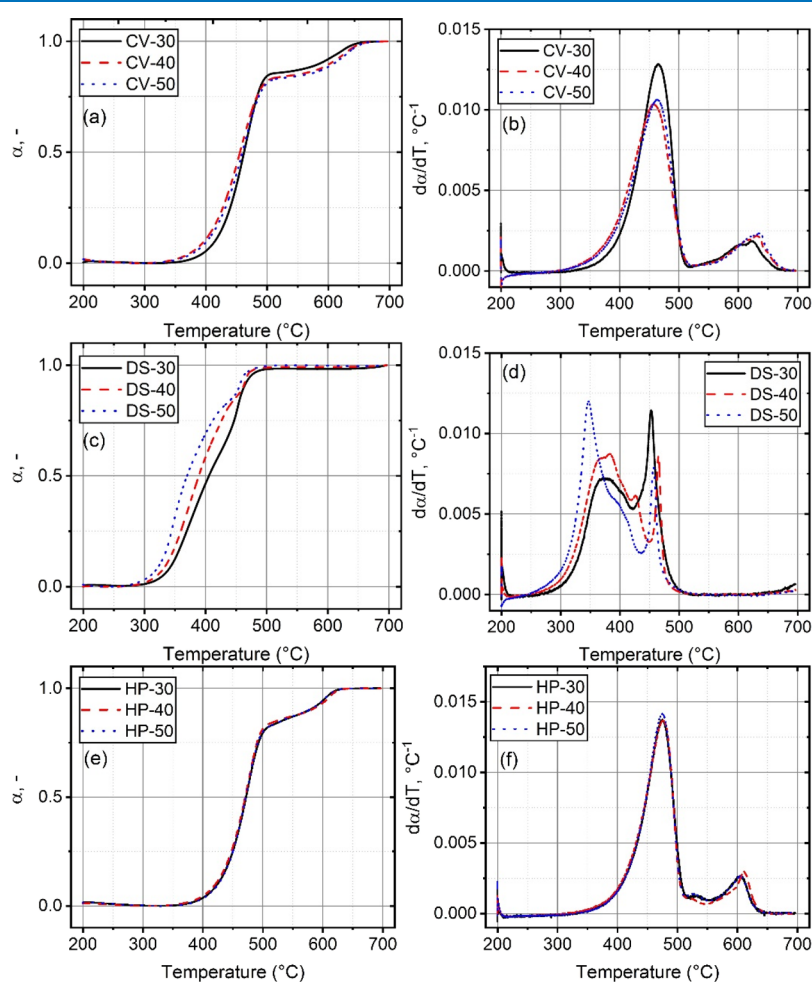

Figure 2. Evolution curves of α and $d\alpha/dT$ with temperature for the biochar combustion process. (a,b) CV biochar, (c,d) DS biochar, and (e,f) HP biochar. Note that the numbers in the legend indicate the three different pyrolysis heating rates to produce the biochar samples.
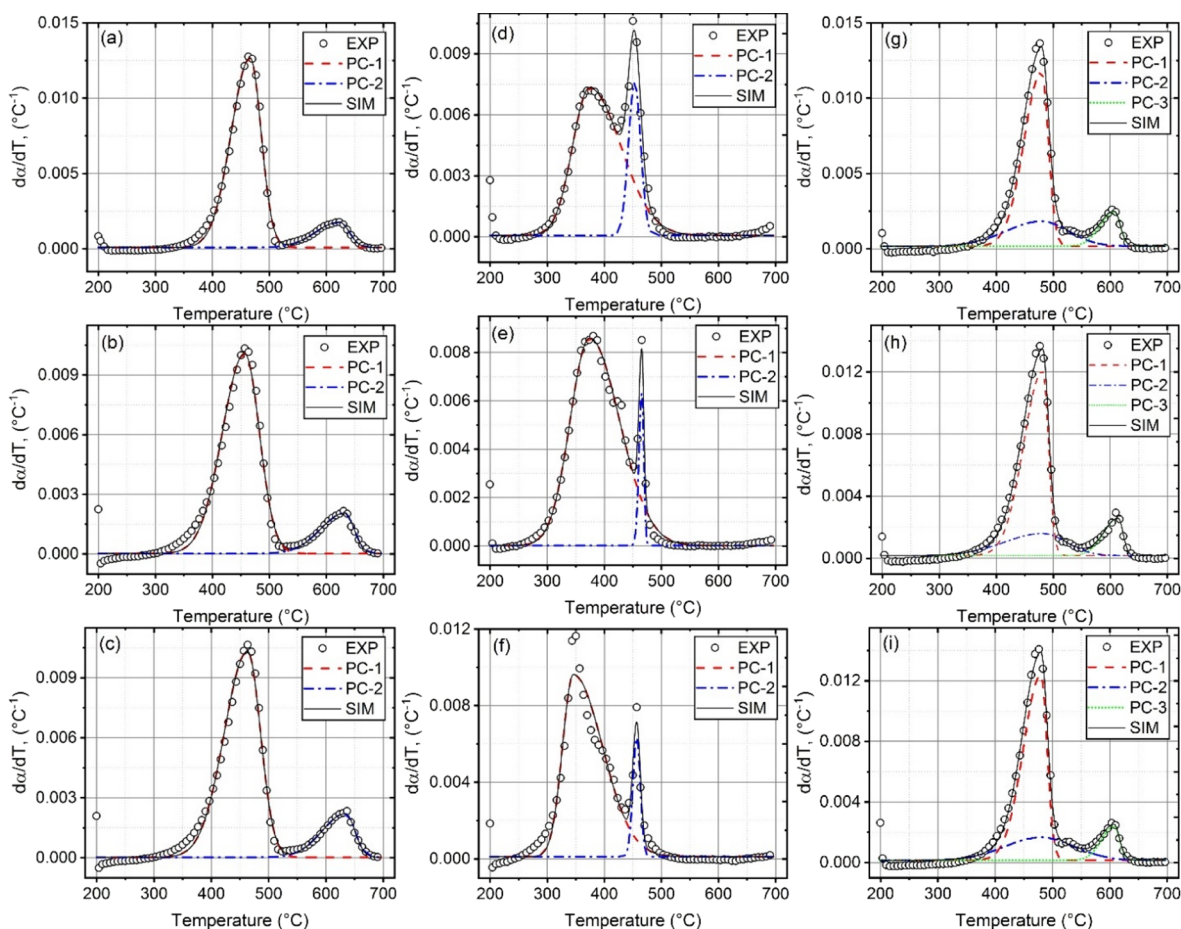
Figure 3. Deconvolution analysis of $d\alpha/dT$ evolution curves for the biochar combustion process. (a) CV-30, (b) CV-40, (c) CV-50, (d) DS-30, (e) DS-40, (f) DS-50, (g) HP-30, (h) HP-40, and (i) HP-50.

Table 3. Ignition and Burnout Temperatures (T_i and T_o) as well as the Simulation Results of the Bi-Gaussian Model

sample	pseudo-component	T_i (°C)	T_O (°C)	y_0 (°C^{-1})	H (°C^{-1})	T_p (°C)	w_1 (°C)	w_2 (°C)	χ^2	R^2
CV-30	PC-1	423.82	490.85	9.39×10^{-5}	0.01258	465.95	33.174	19.519	7.8829×10^{-8}	0.99316
	PC-2	570.65	644.07	9.39×10^{-5}	0.00169	622.84	41.411	17.135		
CV-40	PC-1	407.06	488.78	2.96×10^{-5}	0.01006	456.38	38.998	26.008	1.0402×10^{-7}	0.98769
	PC-2	577.99	653.48	2.96×10^{-5}	0.00203	632.42	42.627	16.199		
CV-50	PC-1	412.01	491.81	2.48×10^{-5}	0.0103	463.08	40.378	22.724	8.5221×10^{-8}	0.99017
	PC-2	582.14	654.60	2.48×10^{-5}	0.00219	634.33	40.978	16.165		
DS-30	PC-1	335.72	442.65	7.24×10^{-5}	0.00725	373.99	29.851	54.869	9.1235×10^{-8}	0.98921
	PC-2	438.5	466.75	7.24×10^{-5}	0.00749	453.11	10.836	10.460		
DS-40	PC-1	331.09	439.62	1.60×10^{-5}	0.00858	373.92	33.880	52.461	5.1772×10^{-8}	0.99390
	PC-2	459.89	470.58	1.60×10^{-5}	0.00627	465.57	4.959	3.496		
DS-50	PC-1	321.52	409.94	1.17×10^{-4}	0.00951	345.65	19.108	50.787	2.8449×10^{-7}	0.96924
	PC-2	447.12	465.16	1.17×10^{-4}	0.00616	456.81	6.844	6.227		
HP-30	PC-1	440.58	495.16	1.80×10^{-4}	0.01156	479.31	30.779	12.069	6.2395×10^{-8}	0.99466
	PC-2	401.8	538.09	1.80×10^{-4}	0.00166	479.31	62.109	46.957		
	PC-3	575.92	619.81	1.80×10^{-4}	0.00229	606.85	24.666	10.421		
HP-40	PC-1	438.66	495.00	1.76×10^{-4}	0.01186	481.25	33.498	10.172	5.2091×10^{-8}	0.99560
	PC-2	397.17	533.31	1.76×10^{-4}	0.00143	481.25	67.504	41.663		
	PC-3	581.19	624.76	1.76×10^{-4}	0.0024	613.78	25.482	8.459		
HP-50	PC-1	440.74	493.88	1.54×10^{-4}	0.0122	479.61	30.763	10.912	6.0165×10^{-8}	0.99507
	PC-2	401.32	551.34	1.54×10^{-4}	0.0015	479.61	62.505	57.393		
	PC-3	578.95	619.49	1.54×10^{-4}	0.00224	607.32	22.074	9.511		

component is treated individually for the kinetic analysis in this work.

3.2. Deconvolution. The complex combustion of algal biochar is further analyzed by using the peak deconvolution

Table 4. Kinetic Models Used in This Work

model	nomenclature	$f(\alpha)$	$g(\alpha)$
Mampel's first order	F1	$1 - \alpha$	$-\ln(1 - \alpha)$
Avrami−Erofeev's nucleation	A3	$3(1 - \alpha)[-\ln(1 - \alpha)]^{2/3}$	$[-\ln(1 - \alpha)]^{1/3}$
3-D diffusion	D3	$3/2(1 - \alpha)^{2/3}[1 - (1 - \alpha)^{1/3}]^{-1}$	$[1 - (1 - \alpha)^{1/3}]^2$
shrinking core	R3	$3(1 - \alpha)^{2/3}$	$1 - (1 - \alpha)^{1/3}$

technique. Based on the discussion in the previous subsection, CV and DS biochars are assumed to have two pseudo-components (i.e., PC-1 and PC-2), while HP biochar has three pseudo-components (i.e., PC-1, PC-2, and PC-3). Figure 3 depicts the deconvolution analysis of biochar combustion data for all algal biochar samples. Moreover, for each pseudo-component of biochars, the optimized parameters required for the bi-Gaussian model (eq 9) are assembled in Table 3.

For CV biochar, the peaks of the two pseudo-components are located quite far apart. When the pyrolysis heating rate increases from 30 to 50 °C/min, the peak temperature (T_p) of the first pseudo-component (PC-1) decreases first and then increases. However, the T_p of the second pseudo-component (PC-2) increases monotonically from 622.84 to 634.33 °C, implying that increasing the pyrolysis heating rate makes the combustion of CV biochar more difficult at higher temperatures. For DS biochar, the peaks of PC-1 show a shift toward lower temperatures as T_p reduces from 373.99 to 345.65 °C as the pyrolysis heating rate increases from 30 to 50 °C/min, suggesting an ease in the initial combustion of DS biochar produced at a higher pyrolysis heating rate. Meanwhile, for HP biochar, as seen from Figure 3g−i, the overall reaction can be divided into three stages, and PC-2 is included due to a small peak observed between 510 and 550 °C in the $d\alpha/dT$ curve of HP biochar. Interestingly, the T_p of all pseudo-components of HP biochar remain almost consistent with increasing the pyrolysis heating rate.

3.3. Activation Energy Analysis. Using the Coats−Redfern method (eq 7), the activation energies were calculated for all the pseudo-components of each biochar sample. As shown in Table 4, four common solid-state reaction kinetic models, i.e., Mampel's first-order model, Avrami−Erofeev's nucleation model, 3-D diffusion model, and shrinking core model, are used to obtain the values of activation energies. These E_a values are estimated between the ignition and burnout temperatures. As sketched in Figure 4, the ignition temperature T_i is determined by intersecting the tangent passing through the T_p point on the TG curve with the initial baseline. Similarly, the burnout temperature T_o is found by intersecting the same tangent with the final baseline.[23,30] Note that the ignition and burnout temperatures for all the pseudo-components of each biochar sample are also listed in Table 3.
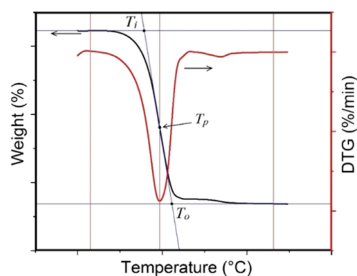

Figure 4. Schematic diagram of the locations of ignition (T_i), peak (T_p), and burnout (T_o) temperatures.

Figure 5 presents the activation energies for all pseudo-components of each biochar sample using four different kinetic
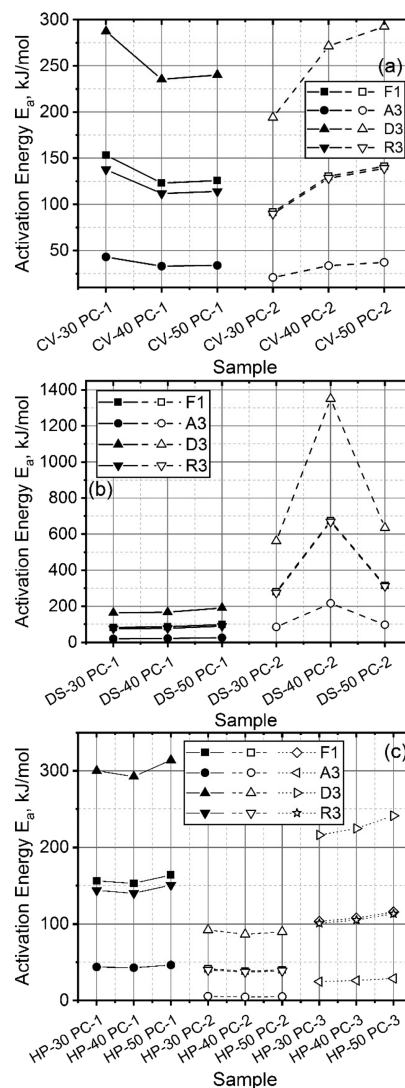

Figure 5. Activation energy distribution for the pseudo-components of each biochar sample using four different kinetic models. (a) CV biochar, (b) DS biochar, and (c) HP biochar.

models. Since E_a is considered the minimum energy required for the reaction to begin, a higher E_a signifies a lower quality of the fuel in some sense. Clearly, the highest E_a values are seen for the D3 model followed by the F1, R3, and A3 models. Koçer et al.[15] also found that the D3 model gave the highest E_a values during pyrolysis of CV. Although the E_a values for different kinetic models are largely different from each other, their evolving trend with the pyrolysis heating rate seems to be independent of the kinetic model.

For CV biochar, with increasing the pyrolysis heating rate, the E_a of its two pseudo-components behaves in different

manners. The E_a of PC-1 decreases from 287.43 to 240.15 kJ/mol for the D3 model, indicating that less heat is required for the combustion of PC-1 when biochar is generated at higher heating rates. Conversely, the E_a of PC-2 increases from 194.05 to 292.77 kJ/mol for the D3 model. For DS biochar, the E_a of PC-1 increases with the pyrolysis heating rate, meaning that more energy is needed for the reaction. However, the increase is moderate as it increases from 163.73 to 191.32 kJ/mol for the D3 model, 82.64 to 98.43 kJ/mol for the F1 model, and 20.23 to 25.74 kJ/mol for the A3 model. In addition, the E_a of its PC-2 increases sharply first and then decreases. For HP biochar, an overall increase in the E_a of PC-1 and PC-3 is observed, whereas that of PC-2 is nearly constant with increasing the pyrolysis heating rate. Specifically, the E_a of PC-1 increases from 299.95 to 313.92 kJ/mol for the D3 model. The E_a of PC-3 also enhances gradually from 216.17 to 241.37 kJ/mol for the D3 model and from 24.81 to 28.94 kJ/mol for the A3 model. As a result, the overall energy requirement for the combustion of HP biochar increases as the pyrolysis heating rate increases.

As shown in Table 5, almost all the samples show a net increase in the activation energy as the pyrolysis heating rate

Table 5. Differences Observed in the Activation Energies of Biochar Combustion Using the Diffusion Model D3 at Different Pyrolysis Heating Rates

sample	E_a (kJ/mol) at $\beta = 30$ °C/min	E_a (kJ/mol) at $\beta = 50$ °C/min	difference
CV PC-1	287.43	240.15	−16.45%
CV PC-2	194.05	292.77	50.87%
DS PC-1	163.73	191.32	16.85%
DS PC-2	561.46	634.98	13.09%
HP PC-1	299.95	313.92	4.66%
HP PC-2	92.36	89.89	−2.67%
HP PC-3	216.17	241.37	11.66%

increases from 30 to 50 °C/min, indicating that more energy is required for biochar combustion if it is formed at higher heating rates.

3.4. Combustibility Index. There are many characteristic parameters that can define the performance of a combustion process. Table 6 lists the maximum and mean mass loss rates, i.e., $(d\alpha/dT)_{max}$ and $(d\alpha/dT)_{mean}$, for each pseudo-component. Note that the ignition and burnout temperatures for all the pseudo-components of each biochar are already summarized in Table 3. High ignition and burnout temperatures indicate that the reaction starts at a high temperature, thus requiring more energy for combustion. Meanwhile, large maximum and mean mass loss rates denote good combustion quality. Therefore, these parameters can be combined into a single parameter called the combustibility index (S_n), which defines the combustion quality.[43,44]

$$S_n = \frac{\left(\frac{d\alpha}{dT}\right)_{max} \times \left(\frac{d\alpha}{dT}\right)_{mean}}{T_i^2 \times T_o} \quad (11)$$

Note that a greater S_n value generally stands for a better combustion process. Figure 6 shows the S_n for all the pseudo-components of various biochar samples. Clearly, compared to PC-2 and PC-3, the PC-1 of all biochar samples have the highest S_n values, indicating a better combustion quality of algal biochars at a low temperature. Meanwhile, the much

Table 6. The Maximum and Mean Weight Loss Rates

| sample	pseudo-component	$(d\alpha/dT)_{max}$	$(d\alpha/dT)_{mean}$
CV-30	PC-1	0.01267	0.00285
	PC-2	0.00178	3.18123×10^{-4}
CV-40	PC-1	0.01009	0.00252
	PC-2	0.00206	3.00694×10^{-4}
CV-50	PC-1	0.01032	0.00253
	PC-2	0.00221	3.08333×10^{-4}
DS-30	PC-1	0.00733	0.00172
	PC-2	0.00756	0.00118
DS-40	PC-1	0.0086	0.00188
	PC-2	0.00629	7.57749×10^{-4}
DS-50	PC-1	0.00962	0.00171
	PC-2	0.00627	9.13184×10^{-4}
HP-30	PC-1	0.01174	0.00246
	PC-2	0.00184	7.56316×10^{-4}
	PC-3	0.00246	3.62341×10^{-4}
HP-40	PC-1	0.01204	0.00253
	PC-2	0.0016	6.72179×10^{-4}
	PC-3	0.00258	3.61434×10^{-4}
HP-50	PC-1	0.01235	0.00253
	PC-2	0.00167	7.19271×10^{-4}
	PC-3	0.00239	3.1502×10^{-4}
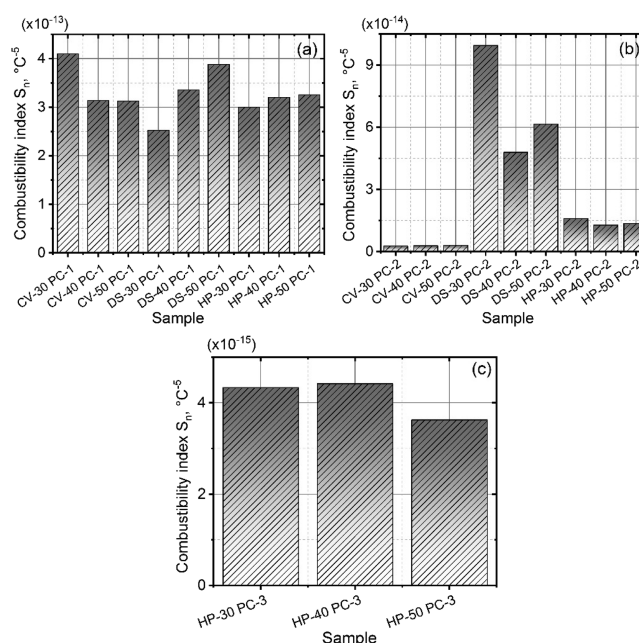
Figure 6. Combustibility index S_n for the pseudo-components of all algal biochar samples. (a) PC-1, (b) PC-2, and (c) PC-3.

lower S_n values for PC-2 and PC-3 signify the fact that the combustion performance is low at a high temperature, probably due to ash formation. In addition, as seen from Figure 6a, as the pyrolysis heating rate increases, the S_n for the PC-1 of CV biochar reduces from 4.10×10^{-13} to 3.13×10^{-13} °C^{-5}, whereas the S_n for the PC-1 of DS and HP biochars monotonically increase from 2.53×10^{-13} to 3.88×10^{-13} °C^{-5} and 3.00×10^{-13} to 3.26×10^{-13} °C^{-5}, respectively. This implies that the combustion performance of the PC-1 of CV biochar is reduced, but those of DS and HP biochars are improved with increasing the pyrolysis heating rate. From Figure 6b, the S_n for the PC-2 of CV biochar increases from 2.70×10^{-15} to 3.07×10^{-15} °C^{-5}, suggesting that the

combustion performance is improved. In contrast, the S_n for the PC-2 of DS biochar decreases from 9.94×10^{-14} to 6.16×10^{-14} °C^{-5}, and for the PC-2 of HP biochar, it reduces from 1.60×10^{-14} to 1.35×10^{-14} °C^{-5}, indicating an overall decrease in the combustion quality of these pseudo-components. Regarding the S_n for the PC-3 of HP biochar, with increasing the pyrolysis heating rate, a small initial enhancement and then a reduction are observed, although the variation is not too significant (Figure 6c).

4. CONCLUSIONS

This work examined the nonisothermal combustion of three algal biochar samples using the multiple component method. Raw algal biomasses were first pyrolyzed at three different heating rates (i.e., 30, 40, and 50 °C/min) to obtain the biochars. Biochar combustion was performed in the temperature range of 200 to 700 °C at a heating rate of 5 °C/min. The results indicated the presence of multiple reactions that appeared to be decomposing as individual parallel processes. Therefore, the bi-Gaussian model was adopted to resolve the global reaction into multiple pseudo-components using the peak deconvolution method. CV and DS contain two pseudo-components (PC-1 and PC-2), and HP contains three pseudo-components (PC-1, PC-2, and PC-3). As the pyrolysis heating rate increases, CV biochar requires more heat at higher temperatures since the peak temperature of CV's PC-2 increases from 622.84 to 634.33 °C. In contrast, the initial combustion of DS biochar requires less heat as the peak temperature of DS's PC-1 declines from 373.99 to 345.65 °C. In addition, no considerable change is observed in the peak temperatures of HP's pseudo-components.

Activation energies (E_a) were evaluated for all pseudo-components of each biochar sample by using the Coats−Redfern method as well as four different reaction models. The highest E_a values are seen for the diffusion model followed by the order-based, shrinking core, and nucleation models. Although the E_a values for different kinetic models are different, their evolving trend with the pyrolysis heating rate seems to be consistent. By using the diffusion model, the E_a of CV's PC-1 decreases from 287.43 to 240.15 kJ/mol, that of CV's PC-2 increases from 194.05 to 292.77 kJ/mol, and that of DS's PC-1 increases from 163.73 to 191.32 kJ/mol with increasing the pyrolysis heating rate.

In addition, the combustibility index also reveals that the combustion performance of algal biochar deteriorates toward a high temperature. Apart from the PC-1 of DS and HP and the PC-2 of CV, all other pseudo-components broadly show a significant reduction in the combustibility index, suggesting a decrease in the combustion quality of algal biochars as the pyrolysis heating rate increases.

■ AUTHOR INFORMATION

Corresponding Author

    Xiaoke Ku − *Department of Engineering Mechanics and State Key Laboratory of Clean Energy Utilization, Zhejiang University, 310027 Hangzhou, China;* ⊙ orcid.org/0000-0002-2182-3933; Phone: +8657187952221; Email: xiaokeku@zju.edu.cn

Authors

    Vikul Vasudev − *Department of Engineering Mechanics, Zhejiang University, 310027 Hangzhou, China*

    Jianzhong Lin − *Department of Engineering Mechanics, Zhejiang University, 310027 Hangzhou, China*

Complete contact information is available at:
https://pubs.acs.org/10.1021/acsomega.1c02493

Notes

The authors declare no competing financial interest.

■ REFERENCES

(1) Morgan, T. J.; Youkhana, A.; Turn, S. Q.; Ogoshi, R.; Garcia-Pérez, M. Review of Biomass Resources and Conversion Technologies for Alternative Jet Fuel Production in Hawai'i and Tropical Regions. *Energy Fuels* **2019**, *33*, 2699−2762.

(2) Potters, G.; Van Goethem, D.; Schutte, F. Promising Biofuel Resources : Lignocellulose and Algae Early Thinking on Biofuels Vegetable Oils : The First Generation Biofuels, The Downsides of Biofuels. *Nat. Educ.* **2010**, *3*, 14.

(3) Vasudev, V.; Ku, X.; Lin, J. Kinetic Study and Pyrolysis Characteristics of Algal and Lignocellulosic Biomasses. *Bioresour. Technol.* **2019**, *288*, 121496.

(4) Yuan, T.; Tahmasebi, A.; Yu, J. Comparative Study on Pyrolysis of Lignocellulosic and Algal Biomass Using a Thermogravimetric and a Fixed-Bed Reactor. *Bioresour. Technol.* **2015**, *175*, 333−341.

(5) Cerciello, F.; Apicella, B.; Russo, C.; Cortese, L.; Senneca, O. Effects of Pressure on Lignocellulosic Biomass Fast Pyrolysis in Nitrogen and Carbon Dioxide. *Fuel* **2021**, *287*, 119604.

(6) Brindhadevi, K.; Anto, S.; Rene, E. R.; Sekar, M.; Mathimani, T.; Thuy Lan Chi, N.; Pugazhendhi, A. Effect of Reaction Temperature on the Conversion of Algal Biomass to Bio-Oil and Biochar through Pyrolysis and Hydrothermal Liquefaction. *Fuel* **2021**, *285*, 119106.

(7) Gautam, R.; Vinu, R. Reaction Engineering and Kinetics of Algae Conversion to Biofuels and Chemicals: *Via* Pyrolysis and Hydrothermal Liquefaction. *React. Chem. Eng.* **2020**, *5*, 1320−1373.

(8) Li, J.; Qiao, Y.; Zong, P.; Wang, C.; Tian, Y.; Qin, S. Thermogravimetric Analysis and Isoconversional Kinetic Study of Biomass Pyrolysis Derived from Land, Coastal Zone, and Marine. *Energy Fuels* **2019**, *33*, 3299−3310.

(9) Kadam, K. L. Environmental Implications of Power Generation via Coal-Microalgae Cofiring. *Energy* **2002**, *27*, 905−922.

(10) Bach, Q. V.; Chen, W. H. Pyrolysis Characteristics and Kinetics of Microalgae via Thermogravimetric Analysis (TGA): A State-of-the-Art Review. *Bioresour. Technol.* **2017**, *246*, 88−100.

(11) Kim, D. W.; Koriakin, A.; Jeong, S. Y.; Lee, C. H. Co-Processing of Heavy Oil with Wood Biomass Using Supercritical m-Xylene and n-Dodecane Solvents. *Korean J. Chem. Eng.* **2017**, *34*, 1961−1969.

(12) Vasudev, V.; Kumar, A.; Saini, V.; Dondapati, R. S. Analytical Estimation for Temperature Dependent Transport Properties of Supercritical Jet Fuel Surrogate. *Int. J. Mech. Eng. Technol.* **2017**, *8*, 1292−1298.

(13) Michalak, I.; Baśladyńska, S.; Mokrzycki, J.; Rutkowski, P. Biochar from a Freshwater Macroalga as a Potential Biosorbent for Wastewater Treatment. *Water* **2019**, *11*, 4−6.

(14) Yu, K. L.; Lau, B. F.; Show, P. L.; Ong, H. C.; Ling, T. C.; Chen, W. H.; Ng, E. P.; Chang, J. S. Recent Developments on Algal Biochar Production and Characterization. *Bioresour. Technol.* **2017**, *246*, 2−11.

(15) Koçer, A. T.; Mutlu, B.; Özçimen, D. Investigation of Biochar Production Potential and Pyrolysis Kinetics Characteristics of Microalgal Biomass. *Biomass Convers. Biorefin.* **2020**, *10*, 85−94.

(16) Elnour, A. Y.; Alghyamah, A. A.; Shaikh, H. M.; Poulose, A. M.; Al-Zahrani, S. M.; Anis, A.; Al-Wabel, M. I. Effect of Pyrolysis Temperature on Biochar Microstructural Evolution, Physicochemical Characteristics, and Its Influence on Biochar/Polypropylene Composites. *Appl. Sci.* **2019**, *9*, 1149.

(17) Li, T.; Wang, L.; Ku, X.; Güell, B. M.; Løvås, T.; Shaddix, C. R. Experimental and Modeling Study of the Effect of Torrefaction on the Rapid Devolatilization of Biomass. *Energy Fuels* **2015**, *29*, 4328−4338.

(18) Ku, X.; Li, T.; Løvås, T. Effects of Particle Shrinkage and Devolatilization Models on High-Temperature Biomass Pyrolysis and Gasification. *Energy Fuels* **2015**, *29*, 5127−5135.

(19) Jayaraman, K.; Kök, M. V.; Gökalp, I. Combustion Mechanism and Model Free Kinetics of Different Origin Coal Samples: Thermal Analysis Approach. *Energy* **2020**, *204*, 117905.

(20) Emre Altun, N.; Hicyilmaz, C.; Kök, M. V. Effect of Particle Size and Heating Rate on the Pyrolysis of Silopi Asphaltite. *J. Anal. Appl. Pyrolysis* **2003**, *67*, 369−379.

(21) Vyazovkin, S.; Burnham, A. K.; Criado, J. M.; Pérez-Maqueda, L. A.; Popescu, C.; Sbirrazzuoli, N. ICTAC Kinetics Committee Recommendations for Performing Kinetic Computations on Thermal Analysis Data. *Thermochim. Acta* **2011**, *520*, 1−19.

(22) Coats, A. W.; Redfern, J. P. Kinetic Parameters from Thermogravimetric Data. *Nature* **1964**, *201*, 68−69.

(23) Wang, C.; Du, Y.; Che, D. Reactivities of Coals and Synthetic Model Coal under Oxy-Fuel Conditions. *Thermochim. Acta* **2013**, *553*, 8−15.

(24) Jayaraman, K.; Kok, M. V.; Gokalp, I. Thermogravimetric and Mass Spectrometric (TG-MS) Analysis and Kinetics of Coal-Biomass Blends. *Renewable Energy* **2017**, *101*, 293−300.

(25) Hu, M.; Chen, Z.; Wang, S.; Guo, D.; Ma, C.; Zhou, Y.; Chen, J.; Laghari, M.; Fazal, S.; Xiao, B.; Zhang, B.; Ma, S. Thermogravimetric Kinetics of Lignocellulosic Biomass Slow Pyrolysis Using Distributed Activation Energy Model, Fraser-Suzuki Deconvolution, and Iso-Conversional Method. *Energy Convers. Manage.* **2016**, *118*, 1−11.

(26) Sharma, P.; Pandey, O. P.; Diwan, P. K. Non-Isothermal Kinetics of Pseudo-Components of Waste Biomass. *Fuel* **2019**, *253*, 1149−1161.

(27) da Silva, J. C. G.; de Albuquerque, J. G.; Galdino, W. V. d. A.; de Sena, R. F.; Andersen, S. L. F. Single-Step and Multi-Step Thermokinetic Study−Deconvolution Method as a Simple Pathway for Describe Properly the Biomass Pyrolysis for Energy Conversion. *Energy Convers. Manage.* **2020**, *209*, 112653.

(28) Buys, T. S.; De Clerk, K. Bi-Gaussian Fitting of Skewed Peaks. *Anal. Chem.* **1972**, *44*, 1273−1275.

(29) Gogoi, M.; Konwar, K.; Bhuyan, N.; Borah, R. C.; Kalita, A. C.; Nath, H. P.; Saikia, N. Assessments of Pyrolysis Kinetics and Mechanisms of Biomass Residues Using Thermogravimetry. *Bioresour. Technol. Rep.* **2018**, *4*, 40−49.

(30) Qin, K.; Thunman, H. Diversity of Chemical Composition and Combustion Reactivity of Various Biomass Fuels. *Fuel* **2015**, *147*, 161−169.

(31) Sobek, S.; Werle, S. Kinetic Modelling of Waste Wood Devolatilization during Pyrolysis Based on Thermogravimetric Data and Solar Pyrolysis Reactor Performance. *Fuel* **2020**, *261*, 116459.

(32) Yang, Z.; Zhang, L.; Zhang, Y.; Bai, M.; Zhang, Y.; Yue, Z.; Duan, E. Effects of Apparent Activation Energy in Pyrolytic Carbonization on the Synthesis of MOFs-Carbon Involving Thermal Analysis Kinetics and Decomposition Mechanism. *Chem. Eng. J.* **2020**, *395*, 124980.

(33) Chen, T.; Ku, X.; Lin, J. CFD Simulation of the Steam Gasification of Millimeter-Sized Char Particle Using Thermally Thick Treatment. *Combust. Flame* **2020**, *213*, 63−86.

(34) Sydney, E.B.; Novak, A.C.; de Carvalho, J.C.; Soccol, C.R. Potential Carbon Fixation of Industrially Important microalgae. *In Biofuels from Algae*; Elsevier: Amsterdam, 2019; pp. 67−88.

(35) Sydney, E.B.; Novak, A.C.; de Carvalho, J.C.; Soccol, C.R. Respirometric Balance and Carbon Fixation of Industrially important Algae. *In Biofuels from Algae*; Elsevier: Amsterdam, 2014; pp. 67−84.

(36) Masojídek, J.; Torzillo, G. Mass Cultivation of Freshwater Microalgae. *Reference Module in Earth Systems and Environmental Sciences*; 2014, Elsevier, DOI: 10.1016/B978-0-12-409548-9.09373-8.

(37) Choi, Y. Y.; Joun, J. M.; Lee, J.; Hong, M. E.; Pham, H. M.; Chang, W. S.; Sim, S. J. Development of Large-Scale and Economic PH Control System for Outdoor Cultivation of Microalgae Haematococcus Pluvialis Using Industrial Flue Gas. *Bioresour. Technol.* **2017**, *244*, 1235−1244.

(38) Huang, Y. F.; Lo, S. L. Predicting Heating Value of Lignocellulosic Biomass Based on Elemental Analysis. *Energy* **2020**, *191*, 116501.

(39) Vasudev, V.; Ku, X.; Lin, J. Pyrolysis of Algal Biomass: Determination of the Kinetic Triplet and Thermodynamic Analysis. *Bioresour. Technol.* **2020**, *317*, 124007.

(40) Kök, M. V. Heating Rate Effect on the DSC Kinetics of Oil Shales. *J. Therm. Anal. Calorim.* **2007**, *90*, 817−821.

(41) Angin, D. Effect of Pyrolysis Temperature and Heating Rate on Biochar Obtained from Pyrolysis of Safflower Seed Press Cake. *Bioresour. Technol.* **2013**, *128*, 593−597.

(42) Kök, M. V. An Investigation into the Combustion Curves of Lignites. *J. Therm. Anal. Calorim.* **2001**, *64*, 1319−1323.

(43) Wang, X.; Hu, Z.; Deng, S.; Wang, Y.; Tan, H. Kinetics Investigation on the Combustion of Biochar in O_2/CO_2 Atmosphere. *Environ. Prog. Sustainable Energy* **2015**, *34*, 923−932.

(44) He, X.-M.; Yi, S.; Fu, P.-R.; Zeng, X.-C.; Zhang, D.; Cheng, X.-H. Combustion Reactivity of Biochar and Char Generated from Co-Pyrolysis of Coal and Four Additives: Application in Blast Furnace. *J. Energy Eng.* **2017**, *143*, No. 04016023.